OPTICA QUANTUM

Enabling photonic integrated 3D magneto-optical traps for quantum sciences and applications

Daniel J. Blumenthal,[1,*] Andrei Isichenko,[1] and Nitesh Chauhan[1,2,3]

[1]Department of Electrical and Computer Engineering, University of California Santa Barbara, Santa Barbara, California 93106, USA
[2]Present Address: Time and Frequency Division, National Institute of Standards and Technology, Boulder, Colorado 80305, USA
[3]Present Address: Department of Physics, University of Colorado, Boulder, Colorado 80305, USA
*danb@ucsb.edu

Received 10 June 2024; revised 25 September 2024; accepted 18 October 2024; published 6 December 2024

Cold atoms play an important role in fundamental physics, precision timekeeping, quantum and gravitational sensing, precision metrology, and quantum computing. The three-dimensional magneto-optical trap (3D-MOT) is a fundamental tool used to create large populations of cold atoms and serves as an integral component for a wide range of quantum and atomic experiments. The 3D-MOT employs laboratory-scale laser systems to trap, cool, manipulate, and interrogate atoms and quantum states. Photonic integration has reached a point where it is possible to generate, control, and deliver light to atomic transitions and provides a path to integrated 3D-MOTs. We review progress and discuss potential paths toward integration of 3D-MOT lasers and optics with focus on the ultra-low loss silicon nitride photonic integration platform. We review 3D-MOT technology, building blocks and components, and discuss characteristics of the lasers, optics, and atomic physics package. We discuss how the silicon nitride platform can be used to perform MOT functions including cooling, trapping, and spectroscopy. An illustrative example of a rubidium photonic integrated MOT (PICMOT) is used to describe possible paths forward to integration. We also discuss how photonic integration can support lower temperatures and atom trapping and manipulation in integrated cold-atom platforms for quantum sensing and computing.

https://doi.org/10.1364/OPTICAQ.532260

1. INTRODUCTION

The world of precision atomic and quantum sciences is on a path to undergo a transformation to the chip-scale much like computers of the 1950s. This transformation will improve the experimental reliability, reduce size, weight, and cost, impact quantum performance, and enable new discoveries, capabilities, and applications. Cold-atoms in particular play an important role in areas such as new particle discovery and fundamental physics [1,2], optical clocks and precision timekeeping [3–5], quantum and gravitational sensing, precision metrology [6–11], and quantum computing [12–14]. The magneto-optic trap (MOT) [15] is a fundamental tool used to create and spatially confine cold atoms by balancing the motion of thermal atoms with carefully aligned optical radiation and magnetic forces. The MOT can be implemented in a 1-dimensional (1D-MOT), 2-dimensional (2D-MOT), [16] and 3-dimensional (3D-MOT) [15] geometry or a combination of geometries. The MOT mainly consists of three subsystems: a thermal atom source and vacuum cell called the physics package; the magnetic field delivery; and the laser and optics infrastructure used to generate and manipulate optical signals for trapping, cooling, and delivering this light to the atomic species of interest. Today, there is great interest in new technologies that enable integration and miniaturization of all aspects of the MOT [17].

The 3D-MOT [18] in particular is used to create large populations of cold atoms and serves as an integral component for a wide range of experiments including Bose–Einstein condensates (BECs) [8,19,20], optical tweezers [21,22], 3D lattice trapped atoms [23], and atom-interferometry [24,25]. Today, the 3D-MOT is constructed using complex laboratory-scale laser systems, optical components, and control systems, to trap, cool, manipulate, and interrogate atoms and quantum states. The optical infrastructure for a 3D-MOT occupies table-tops and equipment racks, a large volume of the experiment, with components such as precision lasers, reference cavities, spectroscopy cells, the atomic physics package, light delivery optics, modulators, detectors, and frequency shifters. The laser, optics, and electronics infrastructure must be properly designed to interact with the atoms and desired atomic transitions both in terms of atomic energy levels, alignment to these resonances, and characteristics associated with the quality of the light including frequency, polarization, coherence, phase noise, optical power, and beam spatial properties. These components have seen tremendous progress toward their commercialization and miniaturization. Examples of this include integrated 780 nm semiconductor lasers [26], frequency-doubled telecom lasers with high-performance telecom modulators [27,28], reference cavities [29–31], diffraction grating and metasurface MOT beam

delivery [32–35], and centimeter-scale spectroscopy reference cells [17], to name a few.

In this article we review progress and discuss potential paths forward for miniaturization of the lasers and optics infrastructure of the 3D-MOT through photonic integration. Such integration requires a flexible approach that supports the wide range of wavelengths [36] as well as optical performance parameters and functions specific to the MOT-based experiment, the overall 3D-MOT architecture, and miniaturization paths for the other components and subsystems [17,37]. Additionally, the photonic integration platform ideally must be compatible with complementary metal-oxide semiconductor (CMOS) foundry processes to provide the many benefits of wafer-scale processing. Photonic integration of 3D-MOTs will fundamentally advance the quantum and atomic sciences, transforming cold-atom systems and their application in areas like space-based quantum technologies and gravity mapping, portable atomic clocks and quantum sensors, and scalable quantum computing.

First, we provide a brief review of 3D-MOT technology including how these important tools are built today, their key building blocks and underlying component technologies and discuss key characteristics of the lasers, optics, and atomic physics package, focusing on the rubidium and strontium species. We next review integrated approaches to optical beam delivery for cooling and trapping rubidium including pyramidal MOTs (PMOTs) [38–40], grating MOTs (GMOTs) [32–34], integrated metasurface photonic emitters for strontium MOTs [35,41], and photonic integrated circuit (PIC) waveguide to free space rubidium 3D-MOT beam delivery (PICMOT) investigated by our group [42,43]. Next, we introduce the important topic of integrated lasers that can perform MOT functions including cooling, trapping, spectroscopy, and probing as well as their optical parameters such as wavelength, linewidth, noise, and power. Laser stabilization, using optical reference cavities that are critical for many atomic and quantum systems, is described briefly, including the influence of the laser frequency noise and noise reduction in both cold atom sensors [44] and in computing [45]. We move forward with a summary of integration of these lasers, optical reference cavities, and key MOT functions using the ultra-low loss silicon nitride (SiN) PIC platform [46] with attention to state-of-the-art micro-cavities that can be integrated with the SiN PIC platform. Stepping to the miniaturization of the full 3D-MOT we then briefly cover the latest work in compact atomic cells and atomic physics packages. However, this is a large field in itself; there is other important work that covers the integration and miniaturization of the physics package. For a more comprehensive discussion including methods for cell fabrication and compact vacuum systems, we refer the reader to Ref. [17].

We then use an illustrative example of work done by our group on a rubidium PICMOT [43] based on the SiN platform and the paths forward to full integration of all building blocks and technologies including lasers, spectroscopy, amplitude and frequency modulation, beam delivery and other subsystems used in 3D-MOT experiments and associated atomic, molecular, and optical physics (AMO) experiments. We also discuss what technologies can be used to supply atoms to the integrated 3D-MOT, how the MOT can be augmented to support lower temperatures and advanced particle trapping and manipulation and qubit operations (e.g., sub-Doppler cooling, lattice trapping, programmable optical tweezer arrays) and how this area can be applied to important quantum applications including atom interferometry, quantum optical clocks, frequency references, and quantum sensors. We conclude with a perspective on what is next and new advanced technologies.

2. 3D-MOT TECHNOLOGY OVERVIEW

The cooling and trapping of neutral atoms uses a balance of scattering forces formed by the combination of laser beams and a magnetic field gradient to confine atoms in up to three dimensions. The atoms experience a restoring force that confines them in space and reduces their velocity and therefore their temperature [18]. MOTs are made for a variety of atomic species, and alkali metals such as rubidium and cesium are commonly used because of their relatively simple atomic level schemes. MOTs requiring more complicated laser cooling and trapping schemes are used for species such as strontium-87 to access the narrow 698 nm clock transition [47] and combined with optical lattice trapping to achieve unprecedented clock stability reaching 10^{-18} [3].

Confinement in three dimensions is typically achieved with a six-beam 3D-MOT and its constituent components [Figs. 1(a) and 1(b)]. The requirements of different cold atom applications can be generally translated to the atom number N and cloud temperature in the MOT [48]. For example, the sensitivity of atom interferometry can be limited by the quantum projection noise [48] with a desirable atom number of over one million atoms [49]. The trapped atom number can be increased with larger diameter beams and higher optical powers— a challenge for maintaining a small physics package where the cold atoms live and miniaturizing the lasers and optics since scaling the atom number depends on the beam overlap volume within the physics package [48]. The scattering forces on the atoms must be balanced and sufficiently strong to trap and cool the atoms from the background vapor of the cell. Because the forces are dependent on the propagation directions of the cooling beams, at least four beams, and typically six, are used. The intersection of these beams must also coincide with the null points of the magnetic field gradient within the atomic cell. The cold atom cloud temperature is another important metric, and while millikelvin temperatures are routine, reaching temperatures below the Doppler limit of 150 μK (e.g., for Rb) requires additional laser cooling techniques to reach the desired microkelvin regime required for long interrogation times in atom interferometry, optical tweezer-based experiments, and high-fidelity quantum computation. Such experiments utilize the 3D-MOT as the basic cold atom source and then employ layers of sophisticated laser cooling technique to reach these sub-Doppler temperatures such as polarization gradient cooling [50], Raman cooling [51], and optical lattice traps [52]. Even lower temperatures and more sophisticated laser cooling techniques such as evaporative cooling are required for BEC and quantum degeneracy experiments [53].

The key 3D-MOT functions and subsystems, highlighted in Fig. 1(a) include (i) the atom source and vacuum chamber, (ii) laser signal generation, frequency control, modulation, and stabilization, (iii) atomic saturation spectroscopy and lock, (iv) magnetic field control, (v) beam gating, intensity control, and timing/sequencing, and (vi) cooling, trapping, repump, and probe beam delivery. The atom source is typically located inside the vacuum chamber and produces neutral atoms at a steady rate using a resistively heated atomic oven, with smaller

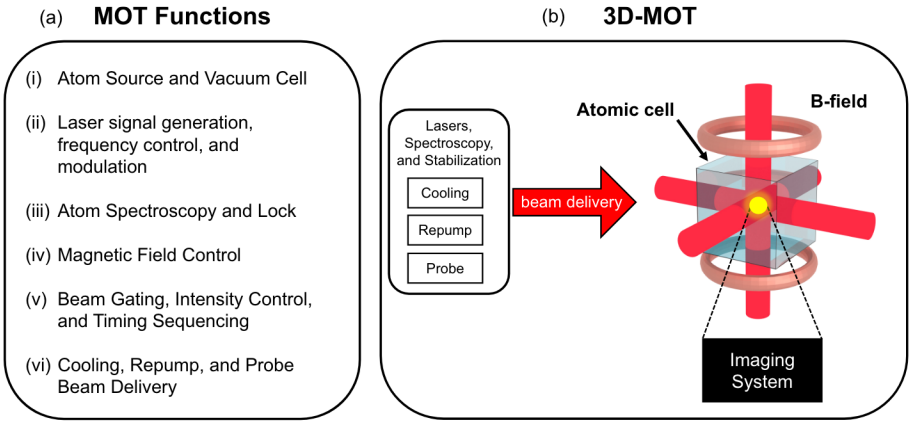

Fig. 1. (a) 3D-MOT functions and (b) an example of the beam delivery in a six beam 3D-MOT configuration.

designs utilizing an atom pill source activated with a high-power laser. The magnetic field is generated using electrical coils arranged in an anti-Helmholtz configuration or alternative magnetic field geometries [17,54] to create a quadrupole trap. The laser subsystem has cooling, repump, and probe signals whose frequencies are aligned to an external atomic reference such as saturation absorption spectroscopy (SAS). Finally, other bulk-optic free space components such as acousto-optic modulators, wave plates, and photodiodes are used to adjust the cooling laser frequency, polarization, and enable locking of optical signals to optical reference cavities and optical atomic transitions. Once the laser frequencies and their control are prepared, the beams are routed to the physics package and split into three entry points, then directed to retroreflector mirrors that back-reflect each beam to form the total six beam configuration [Fig. 1(b)]. The routing, expansion, and splitting of these beams is traditionally achieved using free-space optics. Alternatively, the atom trapping and cooling can be divided into multiple stages. For example, 2D-MOTs can create confinement in two dimensions, allowing a high flux atomic beam to enter a 3D-MOT for a final cooling step.

3. BEAM DELIVERY

Over the last few years there has been progress on miniaturization and integration of the optics for laser beam delivery to the atomic physics package, including splitting, routing, and overlapping the trapping beams. These approaches generally falling in the following categories: metasurface MOT

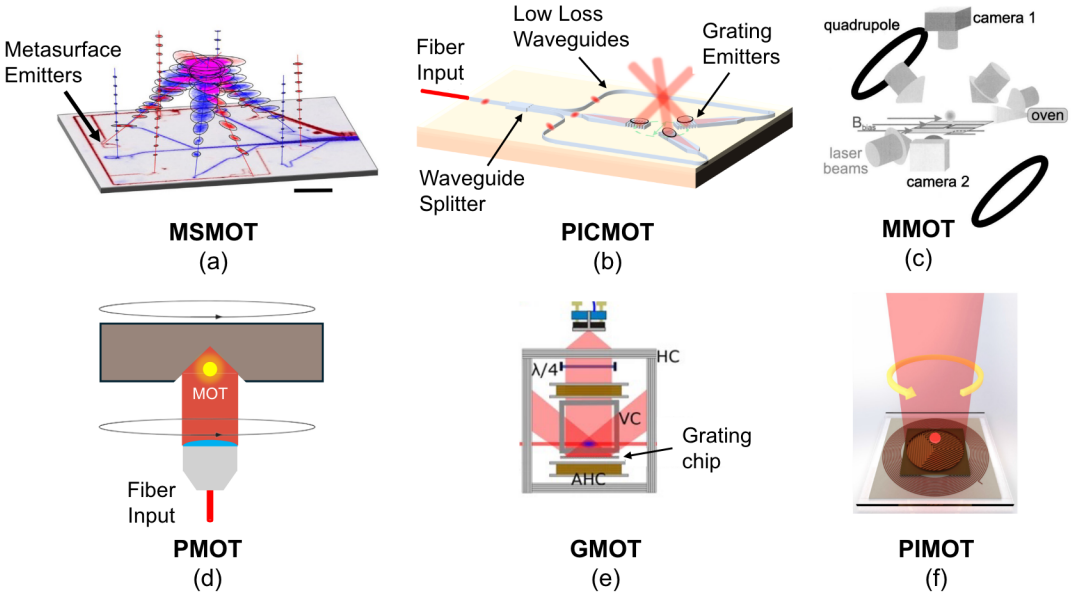

Fig. 2. Compact and integrated 3D-MOT beam delivery approaches. (a) Metasurface MOT – MSMOT [35]. C. Ropp *et al.* Light Sci Appl 12, 83 (2023). Licensed under CC BY 4.0 (https://creativecommons.org/licenses/by/4.0/). (b) Photonic integrated circuit MOT – PICMOT [43]. A. Isichenko *et al.* Nat Commun 14, 3080 (2023). Licensed under CC BY 4.0 (https://creativecommons.org/licenses/by/4.0/). (c) Mirror MOT – MMOT [65]. Reprinted (Fig. 2) with permission from [R. Folman *et al.*, "Controlling Cold Atoms using Nanofabricated Surfaces: Atom Chips," Phys. Rev. Lett. **84**, 4749–4752 (2000).] Copyright (2020) by the American Physical Society. (d) Pyramid MOT – PMOT [39]. (e) Grating MOT – GMOT [33]. J.P. McGilligan *et al.* Sci Rep 7, 384 (2017). Licensed under CC BY 4.0 (https://creativecommons.org/licenses/by/4.0/). (f) Planar integrated MOT – PIMOT [34]. Reprinted [Fig. 2(a)] with permission from [L. Chen *et al.*, "Planar-Integrated Magneto-Optical Trap," Phys. Rev. Appl. **17**, 034031 (2022).] Copyright (2022) by the American Physical Society.

(MSMOT) [Fig. 2(a)]; photonic integrated circuit MOT (PIC-MOT) [Fig. 2(b)]; mirror MOT (MMOT) [Fig. 2(c)]; pyramid MOT (PMOT) [Fig. 2(d)]; grating MOT (GMOT) [Fig. 2(e)]; and planar integrated MOT (PIMOT) [Fig. 2(f)]. The reflection approaches include the PMOT [39,55] and GMOT [17,32,33] reduce the free space elements and enable a compact MOT. In a PMOT, a single large beam illuminates a hollow reflective pyramidal region to generate three sets of counter-propagating beams. These have reported to trap 30×10^6 atoms [55] and also to generate a beam of cold atoms [56]. In a GMOT, a large single beam illuminates a reflection grating to produce three diffracted beams in a tetrahedral geometry [33] using micro-fabricated gratings. Combining the GMOT with micro-fabricated vacuum cells enables compact scalable MOTs for sensors [17,57]. The metasurface-based MSMOT approach utilizes sub-wavelength feature transmission and reflection structures to replace lenses to perform optimized multi-beam splitting [54] and multi-function optical components that can simultaneously redirect, shape, polarize, and expand an incident beam [58]. More recently, metamaterial gratings illuminated by fibers have been successfully employed to produce centimeter-scale expanding beams for the multiple wavelengths needed for a Sr 3D-MOT [35,59]. Metasurfaces combine advantages of low optical losses, polarization engineering, and beam shaping, with the reconfigurability for different wavelengths and fabrication reproducibility using advanced fabrication techniques like electron beam lithography.

The PICMOT approach [43] (Fig. 2(b)) is capable of multi-component integration of lasers, optics, and MOT functions into a planar fabricated waveguide-based structure in the SiN platform [46]. PIC-based beam delivery been demonstrated in ion trapping using micrometer-sized focusing beams [60,61] and in rubidium MOTs using 320 μm diameter [62] and recently 2.5 mm by 3.5 mm (e^{-2} width) collimated beams [43]. It should be noted that the PICMOT can utilize metasurface technology in both the free-space beam emission directly above the waveguide and for beam retroreflection. A metasurface layer above the waveguide can achieve cooling beam expansion [58] for larger atom numbers, to precisely control divergence angle [59], and to combine different wavelengths [63]. For a six-beam MOT geometry requiring retroreflection, metasurfaces can be used as a planar mirror through single-angle reflection [64], enabling integration with a PIC, vacuum cell, and magnetic field generation in a planar stack and eliminating optical alignment. For the basic beam delivery, on-chip waveguides are coupled to a 1×3 integrated power splitter. The splitter outputs are coupled to three slab-waveguide beam expanders that each illuminate waveguide-to-surface mode gratings that generate multi-millimeter diameter collimated beams off-chip at specific angles that intersect orthogonally 9 mm above the PIC surface at a desired location inside the physics package (Fig. 3). The large-area gratings deliver nearly 1 mW per beam and enable cooling and trapping a MOT cloud of 1.3×10^6 atoms at a temperature near 200 μK.

4. INTEGRATED LASERS, MODULATORS, AND REFERENCE CAVITIES

A fully integrated 3D-MOT will incorporate multiple lasers, each at an atom-defined wavelength with specific power, phase noise, and amplitude noise stability tailored to the species, its transitions, the particular MOT function, and the application. A rubidium (Rb) 3D-MOT and clock or electromagnetic sensing applications, will for example, utilize 780 nm for cooling and repump, 778 nm for the Rb two-photon transition [66], or 480 nm for Rydberg excitation [10]. There is usually the need to tune or scan the laser wavelength, either by direct laser tuning or using external frequency shifters such as acousto-optic modulators (AOMs), to stabilize the laser to an optical reference cavity or an atomic transition or to perform spectroscopy. Such scanning can cover from tens of megahertz to multiple gigahertz to nanometers. Frequency shifting by directly controlling a laser requires consideration of issues such as mode-hop free tuning, linearity of tuning, tuning range, residual amplitude modulation (RAM), and more. Another widely used function is modulation, used to generate sidebands and error signals for control loops to lock the laser to reference cavities and atomic transitions. Modulation can also be used to generate new optical frequencies, to access neighboring atomic transitions, to couple coherent atomic transitions, and for qubit coherence control sequencing. Modulators tend to fall into two categories, the first is for control loops operating in the broadband DC-10s to hundreds of megahertz range, and the second is at higher narrowband radio frequencies (RF) in the hundreds of megahertz to 10 GHz range used to create optical signals at atomic transitions offset from a reference such as a spectroscopy cell.

An important set of parameters are the laser linewidth, phase noise, and frequency stability. These requirements will determine the choice of integrated laser for each wavelength. At a high level, the choices are tied to the particular purpose for that wavelength. Examples include pumping a broad atomic transition, cooling the motion of the atom, light scattering from the atom for imaging, repumping a transition back to the ground state, probing very narrow optical transitions such as for clock operations, or coupling multiple optical state transitions with high coherence and fidelity such as for qubit operations. While a detailed discussion of laser linewidth and phase noise is outside the scope of this article, we provide a brief discussion at this point. Laser linewidth and phase noise can be described in terms of the fundamental or instantaneous linewidth (FLW), the integral linewidth (ILW) of which there are several ways to define, the fractional frequency noise (FFN) also form of carrier jitter, the drift, and the actual phase noise at specific offset frequencies from the carrier or integrated over a range of offset frequencies. The nature and impact of these quantities depends on the nature of the noise (memoryless quantum vacuum-driven or with memory), the averaging interval or frequencies over which the spectral content of light is observed or utilized, how the light is used functionally, and the degree of coherence required. For example, the FLW, which is quantum noise driven, determines the phase noise at high offset frequencies typically greater than 100 kHz or 1 MHz, and can impact the sensitivity of a quantum sensor that is intermodulation distortion limited such an optical clock or atom interferometer, or can produce Fourier transform limited aliasing noise when atoms or qubits are sequenced or pulsed at high frequencies [67]. The material properties of the laser itself and its interaction with the external environment are noise processes with memory that modulate the laser carrier and its phase noise leading to a Voight broadened lineshape. Stabilizing the laser to an external reference cavity involves materials in the reference cavity or its mirrors whose noise fluctuations are quantum photo- or thermally driven, leading to thermorefractive noise (TRN) [68] or photothermal noise (PTN) [69,70] limits on the stabilized laser ILW over are range of offset frequencies

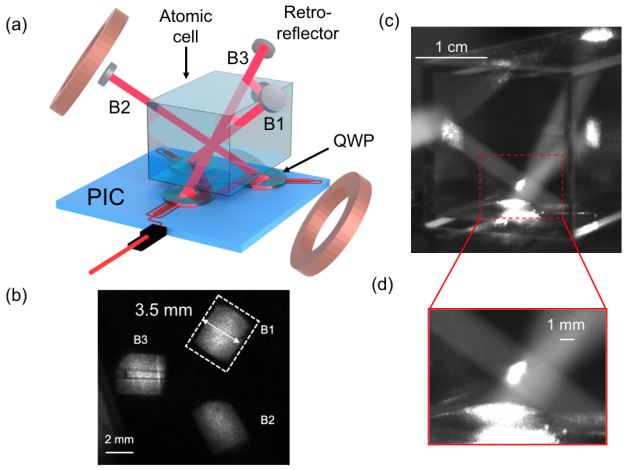

Fig. 3. Photonic-integrated circuit 3D-MOT (PICMOT) [43]. (a) Beam delivery to form a 3D-MOT with the large-area grating emitter PIC. The quarter wave plates (QWPs) convert from linear to circular polarization for MOT formation. (b) PIC beams incident on a plane above the PIC surface. (c) View of the cold atom MOT cloud with a camera from the side of the setup. (d) Zoom-in of the MOT cloud. A. Isichenko *et al.* Nat Commun 14, 3080 (2023). Licensed under CC BY 4.0 (https://creativecommons.org/licenses/by/4.0/).

typically in the 10 Hz to several kilohertz range. The laser FFN and long-term drift are important when stabilizing the laser to an optical transition while the atom or qubit are being prepared. The FFN gives a frequency range and time over which the laser remains within the capture range of feedback loops while disengaged from the atomic or qubit transition and then needs to lock with the transition when the loop is engaged. The long-term drift is the regime where the laser moves out of capture range relative to the open loop cycle of atom or qubit preparation, possibly moving back again cyclically as the environment fluctuates. In the end, a laser system linewidth can be FLW, ILW, FFN, or drift-dominated and details of the phase noise at various offset frequencies can be critical. Other laser parameters important for atomic and quantum applications include relative intensity noise (RIN) and linewidth enhancement factor that couple phase and amplitude modulation. Experiments for cooling, trapping, and probing in rubidium cold atom systems typically use lasers operating in single mode and have integral linewidths below 1 MHz and fundamental linewidths below 50 kHz which is sufficient for resolving and stabilizing to rubidium hyperfine spectroscopy transitions and therefore generating a rubidium MOT.

An alternate approach to the direct drive emission lasers discussed so far are nonlinear optical techniques such as frequency-doubling of telecom laser systems. Such systems have gained attention in the cold atom community due to their compactness relative maturity of the semiconductor gain material. For rubidium, lasers operating at 1560 nm benefit from a mature technology base, with reliable components such as intensity and phase modulators, and semiconductor optical amplifiers in silicon photonics at 1560 nm allows for further miniaturization of these systems [Fig. 4(a i)]. By preparing the light and modulating at 1560 nm, frequency-doubled second harmonic generation (SHG) or octave spanning optical frequency combs [78] can be used to translate this light to the atomic transitions. This approach has been successfully demonstrated with SHG in a cold atom interferometer [27,28] using a silicon photonics system at 1560 nm with separate non-integrated frequency doubling to 780 nm. Recent work on integrated such systems to the chip level have been reported, with the primary difficulty being limited converted optical power at the transition energy [79]. Other approaches include optical parametric oscillation (OPO) frequency converters which hold promise for higher conversion efficiency [80]. To address the conversion efficiency limits of frequency-doubled systems typically require additional optical power using semiconductor optical amplifiers at the target atomic transition wavelength. This gain material would be used anyway as the gain material for direct drive lasers operating directly at the atomic transition such as the important gallium nitride material system for green and blue [81]. For these reasons, the remainder of this paper focuses on "direct-drive" photonic technologies that operate directly at 780 nm rather than frequency doubled approaches. There are a variety of single longitudinal (frequency) mode laser designs to select from that can be integrated on in the Si_3N_4 platform (Fig. 4(a)). Each type delivers different optical performance and characteristics, the choice depending on the intended MOT function for that wavelength. Each laser type can serve as the basic stand-alone lasing element, can serve as the pump for a higher performance laser (e.g., Brillouin laser), or combine with other elements to realize higher level functions. The designs are ordered with decreasing FLW from the top to bottom of Fig. 4(a). The most basic, and typically the lowest performance in terms of linewidth and phase noise are the semiconductor distributed Bragg reflector (DBR) and distributed feedback (DFB) [82] lasers, which have typical ILW of below 1 MHz, and FLW above 10 kHz, are temperature tunable, and can be integrated with the silicon nitride platform [26,83]. The next level of linewidth and noise performance can be achieved with an extended DBR (EDBR) design [Fig. 4(a ii)] by combining an active reflective semiconductor optical amplifier (RSOA) gain chip, that has a bandgap emission at the desired wavelength range, with an extended silicon nitride Bragg reflector [84,85,86] similar on fiber-based demonstrations [87]. At 1550 nm wavelengths these integrated EDBR lasers can reach 2 kHz FLW and 17 kHz ILW through their extended mode volume and are moderately tunable. To further reduce the FLW and provide wider tunability, the widely used table-top external cavity diode laser (ECDL) or external cavity tunable laser (ECTL) designs [Fig. 4(a iii)] can be integrated on-chip using an RSOA of the appropriate bandgap as the gain block for a multi-ring silicon nitride design [88]. Such lasers are capable of reaching 40 kHz ILW [88] and are directly tunable using thermal or stress-optic actuators with the potential for mode hop free operation. The next category of laser provides extremely low FLW through nonlinear noise reduction via optical feedback. Self-injection locked (SIL) lasers [89] illustrated in Fig. 4(a iv), utilize high optical feedback into the primary laser to suppress noise and cause lasing in a single mode. SILs can be realized by coupling low cost Fabry–Perot (FP), or DFB, or DBR lasers, to a highly reflective integrated ring resonator optical cavity that provides strong feedback via Rayleigh backscattering. Under the right conditions the laser operates at a stable point and the fundamental noise of the FP laser is reduced toward the Schawlow–Townes limited linewidth [90] for that particular cavity. Such lasers have been realized in the SiN platform, by coupling the semiconductor laser to an integrated single- or double-bus high-Q ring resonator combined with on-chip phase tuning and splitting to

provide careful control of the SIL process. Silicon nitride waveguide based SIL lasers have been demonstrated in the visible and near-IR (NIR) [91] and short-wave-IR (SWIR) [92,93], achieving FLW as low as 740 mHz at 780 nm and ILW under 864 Hz [94] and 0.6 Hz and 2.3 kHz ILW at 1550 nm [92]. The second type of ultra-low phase noise integrated laser, that also uses nonlinear noise suppression, is the stimulated Brillouin scattering laser (SBL) [95] illustrated in Fig. 4(a v) [96]. Such lasers, based on silicon nitride ultra-high Q ring resonators, utilize photon-phonon interactions, and convert the input pump light to a scattered Stokes output whose fundamental linewidth is multiple orders of magnitude lower in high frequency noise. These lasers are realized by locking a pump laser such as a DFB, EDBR, or ECTL to a Brillouin resonator cavity, typically consisting of a bus-coupled ring or bus-coupled coil. Such integrated SiN lasers have achieved FLW of 70 mHz at 1550 nm and have been demonstrated at a range of atomic and quantum wavelengths with FLW of 24 Hz at 780 nm [97], 12 Hz at 674 nm [98], and 8 Hz 698 nm [99]. Laser frequency noise profiles associated with such ultra-low linewidths have implications for improved atomic system performance such as in high-fidelity neutral atom quantum computing gates and cold atom interferometers and this is discussed further in the "Applications" section of the text. Optical isolation is essential for protecting these semiconductor lasers from detrimental back-reflections that can increase linewidth or cause mode-hopping. This is typically achieved with free-space bulk-optic magnetic isolators providing ~35 dB of isolation. Several different approaches for non-magnetic on-chip isolators have been demonstrated, including acousto-optic modulation in silicon [73], electro-optic modulation in thin-film lithium niobate [72], and optical Kerr nonlinearity in SiN [100]. It has also been shown that lasers consisting of sufficiently high Q resonators can tolerate higher levels of back-reflection [101], such as in the case of heterogeneously integrated self-injection locked lasers [102].

Modulation and frequency shifting are critical to atomic and quantum systems and central to the 3D-MOT operation. The typical bulk-optic components include AOMs for cooling beam detuning, lithium niobate electro-optic modulation for generating gigahertz-frequency sidebands and intensity modulation or shuttering with an AOM, mechanical switch, or semiconductor optical amplifier (SOA) for cloud temperature measurements. Various types of amplitude and frequency modulators are compatible with integration in the silicon nitride platform and are shown in Fig. 4(b). The first two types utilize the stress optic effect, or strain induced tuning via the piezoelectric effect, to change the index of refraction of the optical waveguide and are well matched to amplitude modulation with optically resonant structures. Phase modulators are possible but require long waveguide structures to achieve π phase shifts. Modulation in the DC to tens to hundreds of megahertz can be achieved using PZT modulators [Fig. 4(b i)] deposited on top of low loss silicon nitride waveguides using a planar process [76]. Such modulators operate independently of wavelength, do not affect the optical loss, and are very low energy typically in the tens to 100 nW regime. The PZT modulators shown in [Fig. 4(b i)] are well-matched to atomic and quantum control and locking functions as well as low power DC biasing [76], and moderate tuning speeds for functions like spectroscopy [103]. Higher frequency resonant modulation, at specific frequencies out to gigahertz, can be achieved using etched waveguide structures whose index are controlled with aluminum nitride actuators [Fig. 4(b ii)] [71] that have higher operating frequency than PZT but are not as efficient at lower frequencies and DC. Broadband, high-frequency modulation, such as used to couple multiple atomic transitions, can be achieved using the electrooptic effect in materials like lithium niobate ($LiNbO_3$) [Fig. 4(b iii)]. Thin film $LiNbO_3$ modulators have been demonstrated for atomic functions [104] and can be integrated with silicon nitride photonics using flip chip bonding [105] techniques. Other types of modulators amenable to integration include surface acoustic wave modulators [Fig. 4(b iv)] [106] and Brillouin modulators [Fig. 4(b v)] [107]. Modulation can be classified into direct modulation of the laser cavity and external modulation. Lasers based on one or more high-Q cavities such as an ECTL or SIL can be frequency modulated by cavity resonance tuning. External modulation with resonant single-ring modulators can be realized by stabilizing the modulator to the laser [76] whereas MZI-based modulators are more broadband and applicable to multi-wavelength modulation. Importantly, achieving the highest extinction ratio would involve cascading several coupled high-Q resonators to reach over 80 dB extinction [108].

The third main basic component is the compact or integrated optical reference cavity, used for laser frequency stabilization, linewidth narrowing, and noise reduction for frequencies offset from the carrier in the range of tens of hertz to hundreds of hertz. Such cavities are the mainstay of atomic and quantum experiments are table-top or rack scale and utilize vacuum cavities and environmental isolation and utilize Pound–Drever–Hall (PDH) [109] with proportional integral–derivative (PID) control loops to lock the laser to the reference cavity. There has been great progress in miniaturizing optical reference cavities, using integrated silicon nitride waveguide resonators and coil-resonators [Fig. 4(c i)] [75,110–112], silica microcavities [Fig. 4(c ii)] [29], and vacuum microcavities with silica mirrors [Fig. 4(c iii)] [30,31]. Recent progress in ultra-high Q, $> 100 \times 10^6$, silicon nitride waveguide coil-resonators for laser stabilization include 3-m-long cavities operating directly at 674 nm for the strontium ion clock transition [98], 4 m and 10-m-long 1560 nm cavities that can be used to stabilize light that is frequency doubled for rubidium transitions. Such cavities can achieve linewidth narrowing of 300× with a 600 Hz FLW at 674 nm, and an ADEV stability of $5\times10^{-13}/\sqrt{\tau}$ at 1 s when locked to the $^{88}Sr^+$ ion 0.4 Hz quadrupole [98].

Other important components include integration-compatible visible to NIR photodetectors that can readily support frequencies in the DC to hundreds of megahertz for control loop and lock functions and higher speed photodetectors that can operate in the 1 to 10 GHz range to support beat-note and offset frequency generation. Such photodetectors can be monolithically integrated [113], butt-coupled to the edge of waveguides [114], evanescently coupled to silicon nitride waveguides through flip chip bonding [115], flip chip bonded to waveguide to grating out-couplers [116], and epitaxially grown [117].

5. INTEGRATION PLATFORM

The waveguide integration platform needs to be low loss [118] and transparent in the visible to NIR for many atomic species, whereas other species can require transparency down to the UV. For example, silicon nitride (SiN) waveguides support visible to NIR wavelengths and aluminum oxide (Al_2O_3) can be utilized to cover the UV to visible. Integration of semiconductors and nonlinear optical materials with these waveguide platforms can

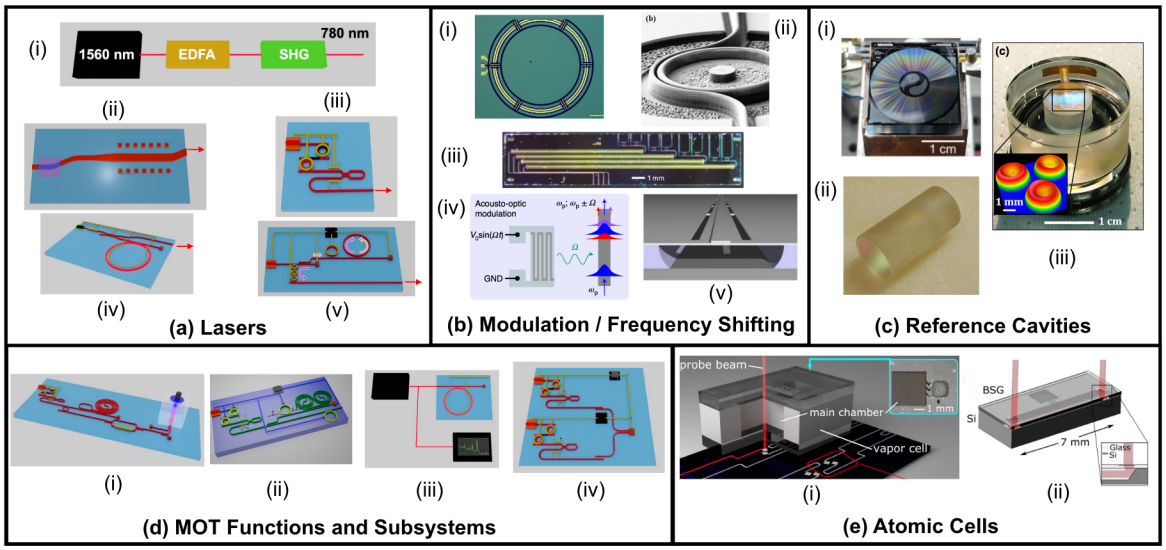

Fig. 4. 3D-MOT integration technologies. (a) Lasers: (i) frequency-doubled C-band lasers; (ii) EDBR; (iii) ECTL; (iv) SIL laser; (v) stimulated Brillouin scattering (SBS) laser with labeled pump (orange) and SBS S1 (purple) light. (b) Modulation and frequency shifting: (i) silicon nitride lead zirconium piezo electric (SiN/PZT); (ii) aluminum nitride (AlN) piezo electric [71]; (iii) lithium niobate ($LiNO_3$) electrooptic [72], reprinted] [Fig. 1(c)] from M. Yu *et al.* Nat. Photon. 17, 666–671 (2023) with permission from Springer Nature; (iv) stimulated Brillouin scattering (SBS) AOM [73], reprinted [Fig. 1(f)] from E. Kittlaus *et al.* Nat. Photonics 15, 43–52 (2021) with permission from Springer Nature; (v) silicon SBS (Si-SBS) [74]. E. Kittlaus *et al.* Nat Commun 8, 15819 (2017), licensed under CC BY 4.0 (https://creativecommons.org/licenses/by/4.0/). (c) Reference cavities: (i) SiN waveguide coil resonator [75]; (ii) silica microcavity (μcavity) [29], reprinted [Fig. 1(a)] from W. Zhang *et al.* Laser & Photonics Reviews 2020, 14, 1900293 with permission from John Wiley and Sons; (iii) vacuum gap (μcavity) [30], reprinted [Fig. 1(c)] with permission from [C. A. McLemore, *et al.*, "Miniaturizing Ultrastable Electromagnetic Oscillators: Sub-10^{-14} Frequency Instability from a Centimeter-Scale Fabry-Perot Cavity," Phys. Rev. Appl. **18**, 054054 (2022).] Copyright (2022) by the American Physical Society. (d) MOT functions and subsystems: (i) SAS; (ii) stabilized lasers [76]; (iii) scanning spectroscopy; (iv) offset frequency and beat-note detection. **(e)** Atomic cells and physics package: (i) waveguide to out-coupler grating to warm vapor rubidium microcell, adapted with permission from [77] © Optical Society of America.; (ii) another microcell geometry [17], J.P. McGilligan *et al.* Review of Scientific Instruments 93.9 (2022), licensed under CC BY 4.0 (https://creativecommons.org/licenses/by/4.0/).

support light emission, detection [113], high speed modulation and optical nonlinearities using materials like thin film $LiNbO_3$ [119]. For example, high bandwidth integrated $LiNbO_3$ modulators can be used to generate sidebands on a ^{87}Rb MOT 780 nm cooling laser to generate a GHz offset repump frequency [18]. Further integration of semiconductor gain materials, with the appropriate bandgap for the desired atomic transition, through butt coupling, photonic wire-bonding, wafer bonding, and epitaxial growth will enable a fully integrated chip where light generation, manipulation, stabilization, delivery, and detection are all achieved on a single chip.

6. HIGHER LEVEL MOT FUNCTION INTEGRATION

The prospects for integrated 3D-MOT building blocks include examples shown in Fig. 4(d). These include integrated saturation spectroscopy which involves laser frequency and intensity stabilization combined with beam delivery to a warm vapor atomic cell [Fig. 4(d i)], laser stabilization [Fig. 4(d ii)] [76], scanning the atomic resonances and aligning the laser to a desired transition [Fig. 4(d iii)], and beat-note detection of offset frequency generation [Fig. 4(d iv)]. Beat note detection plays a key role in monitoring the frequency difference between two lasers for real-time feedback and precision control of one laser frequency with respect to another. These tools enable precise laser frequency control with respect to atomic transitions to sequence through resonant and non-resonant atom probing, essential steps for generating cold atoms in a MOT and for applications such as atom interferometry and quantum computing.

7. COMPACT ATOMIC CELL AND PHYSICS PACKAGE

Scalable, integrated atomic systems will require a compact atomic cell to produce atoms in a vacuum for cooling with photonic circuits. Microfabricated atomic vapor cells have reached a high level of maturity [120] using fabrication techniques similar to that in MEMS devices [Fig. 4(e)]. Unlike conventional glass-blown cells, microfabricated cells are based on anodically bonded silicon-glass structures [17] and enable mass production, greater reliability, and a custom cell geometry. The atomic vapor such as rubidium can be introduced by laser heating a solid alkali pill through a transparent side of the cell. While this technique has been demonstrated for warm vapor atomic (Ref. [77]), cells for cold atom experiment require an ultra-high vacuum level commonly achieved with a liter-scale ion pump. Recent work has successfully integrated micro-ion pumps in a 25 cm^3 chamber [121]. A more detailed discussion about miniaturization of atomic sources and vacuum cells can be found in Ref. [17].

8. FULL MOT INTEGRATION

Full MOT integration will involve combining higher-level func-

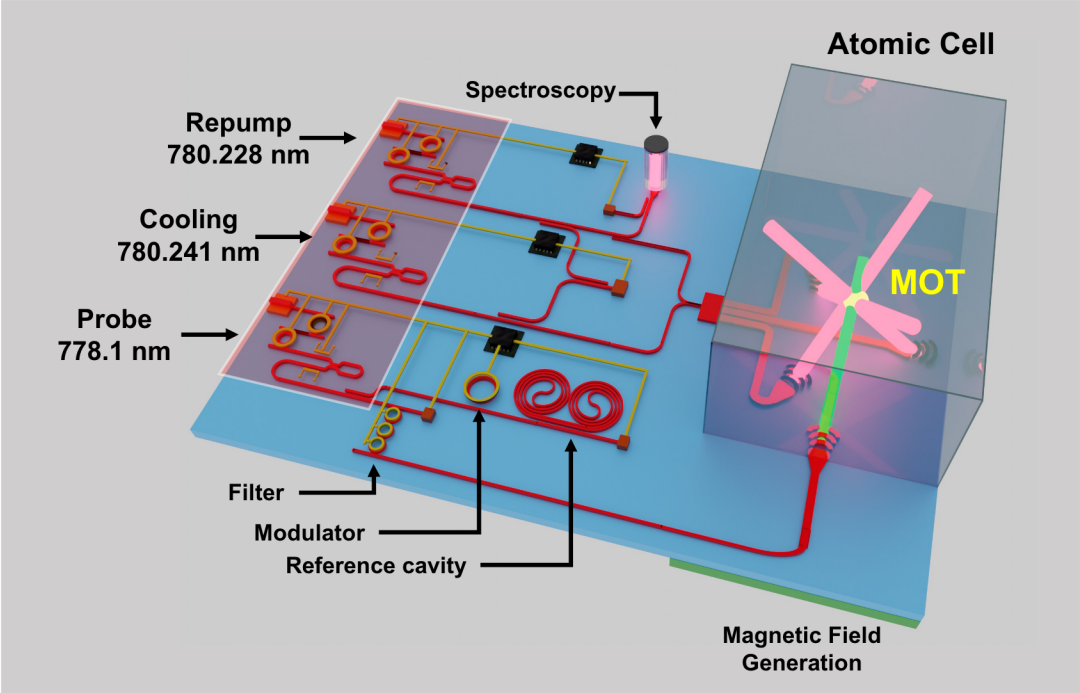

Fig. 5. Illustrative example of a cold atom two-photon atomic clock using integrated lasers for MOT generation and probing and reference cavities, modulators, and filters for probe beam linewidth narrowing and control. The vacuum cell containing the atoms and the magnetic field generation can be planar integrated around the photonic chip. Reprinted with permission of Ref. [43]. A. Isichenko *et al.* Nat Commun 14, 3080 (2023). Licensed under CC BY 4.0 (https://creativecommons.org/licenses/by/4.0/).

tions such as spectroscopy, atomic transition locking, cooling, repump, and probe light generation and modulation, beat note detection and offset frequency locking, and optical gating and pulse sequencing and beam delivery. This transition involves integrating fixed and tunable laser sources, low linewidth and stabilized lasers, modulation, intensity and noise control, high-resolution spectrometers, and detectors onto the same chip. As an example, consider the integration of a cold-atom two-photon clock, as a potential extension of a microwave cold atom clock [122], as illustrated in Fig. 5. Using the common low loss silicon nitride platform, one can integrate rubidium saturation spectroscopy using an ECTL locked to the cold atom repump transition (780.228 nm). The atomic cooling laser (780.241 nm) can be referenced to this line using offset frequency ECTL and beat note detection. The cooling and repump lasers are combined on-chip and delivered to the atomic cell using broad area waveguide to free space beam emitters. To access the two-photon transition, an ultra-low phase noise stabilized laser such as a coil locked ECTL or Brillouin laser can provide an integral linewidth near 1 kHz at 778.1 nm [97]. In this example, the cooling and repump beams are delivered via three gratings to realize the 3D-MOT [43]. The probe beam is delivered via a separate grating to the atom cloud with the ability to shutter the probe with a high extinction ratio filter. While this filter is particularly shown here for the probe beam, it is also crucial for the cooling and repump beams in the clock operation as well as MOT temperature characterization and in atom interferometry. The functions of 420 nm fluorescence detection and microwave-to-optical conversion using an optical frequency comb [37] and magnetic field generation [34] are not shown. The optical frequency comb can also be further integrated using silicon nitride waveguide technology [37,123]. While the spectroscopy cell can be realized using a small millimeter-scale warm vapor cell, the atomic cell will require larger volume and higher vacuum and address issues such as minimizing atom collisions with the walls and how to attach the cell to the PIC using techniques such as anodic or eutectic bonding or laser welding [17]. Other key issue for this high-level of integration will be thermal management and packaging.

Using these technologies, it may be possible to integrate 3D-MOTs for other atomic species that have advantages such as narrower clock transitions and colder atom temperatures. One example is ^{87}Sr neutral strontium atoms, that require two stages of cooling (a red 689 nm MOT and a blue 461 nm MOT) whose lasers must access successive cooling transitions (wavelengths) to finally cool the atoms to a few microkelvin and then use a magic wavelength lattice trap (813 nm) to reduce the motional effects to below 10^{-15}. The probe laser in this case must be extremely low linewidth and high stability to probe the 1 mHz clock transition. Recent work has demonstrated compact laser systems for trapped strontium ions which have a 0.4 Hz transition, including approaches based on frequency doubling and fiber resonators [124] and a PIC-integrated direct-drive 674 nm SBS and coil stabilization reaching sub-600 Hz integral linewidth [98]. The stabilized pump laser in the form of a hybrid ECTL [88] can be readily translated to these visible wavelengths based on the demonstrated resonator performance. An illustrative example of a heterogeneously integrated silicon nitride photonic integrated chip that supports the lasers, optics, and beam delivery for the red and blue MOTs, the magic lattice and the narrow linewidth Brillouin clock transition laser is shown in Fig. 6.

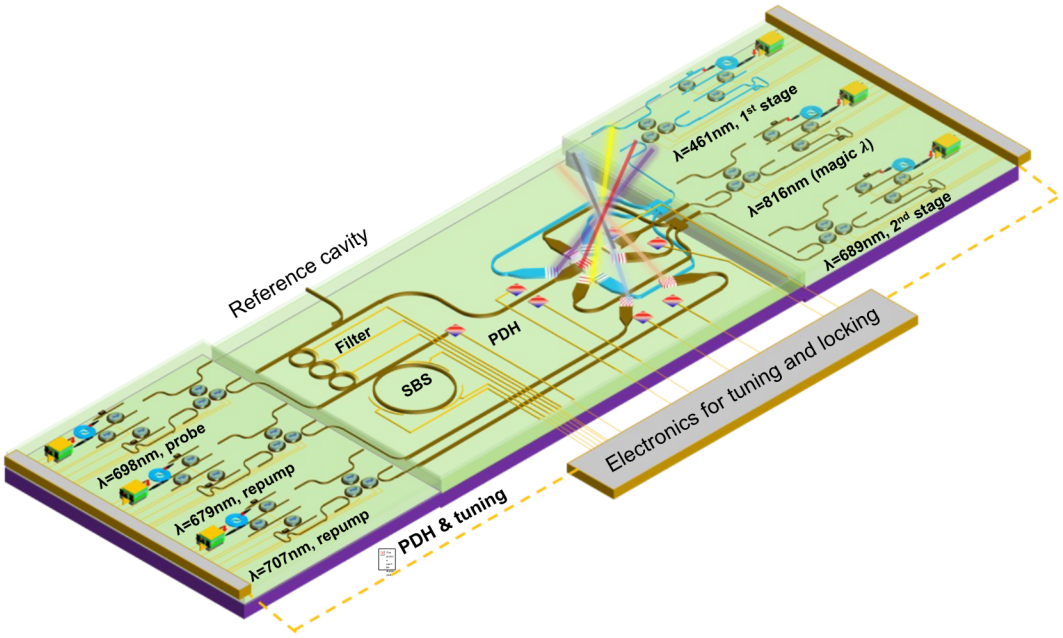

Fig. 6. Illustrative example of a heterogeneously integrated silicon nitride chip for neutral ^{87}Sr cold atom chip to interface with a ^{87}Sr source and cell. Shown are lasers emitting at wavelengths for two-stage (blue and red) MOT cooling, magic wavelength lattice trap, and clock transition probing with a stabilized ultra-narrow linewidth Brillouin laser. Grating beam emitters produce free space beams that can interact with neutral ^{87}Sr in a separate vacuum cell.

9. APPLICATIONS

If integrated 3D-MOTs such as the one proposed in Fig. 6 were to be demonstrated, one could then work toward using this platform to realize cold-atom and quantum information science (QIS) experiments with chip-scale lasers and optical infrastructure. Different types of QIS and quantum experiments require varying cold atom ensemble atom number and temperature performance for the 3D-MOT. For example, sub-Doppler cooling to ensemble temperatures below 20 μK enables certain types of atom interferometry, efficient loading into lattice and optical tweezer traps, and serves as a pre-cooling stage for BECs, and lattice and optical tweezer traps. When the MOT is probed by a precisely controlled 480 nm laser, the atoms can be excited to Rydberg states for Rydberg blockade applications such as quantum computer [125]. This collective excitation allows for precise control of quantum states for computing and sensing [Fig. 7(a)]. These cold atom experiments can be used to implement inertial sensors such as atom interferometers [126] for gravity gradient sensing [127], Rydberg gates for quantum computing [14,128], neutral atom clock arrays [4], 3D trapped neutral atom experiments for fundamental science, including new particle discovery, electric dipole moment (EDM) measurements and dark matter detection. Integration of these experiments and applications will help reduce barriers to entering cold atom science, improve experimental reliability, and enable scaling and improved sensitivity, and portability for field-deployable experiments such as mobile gravity mapping [127] and space-based time-keeping and navigation [129].

As an illustrative example, a rubidium cold atom interferometer (AI) with an atom number over 1×10^6 [48] combined with a sub-Doppler cooling sequence enables increasing the time over which the colder, slowly expanding atom cloud can be interrogated for high-sensitivity inertial measurements. In one approach to sub-Doppler cooling, the cooling laser frequency detuning and power is precisely controlled as the magnetic field is switched off. In a light-pulse AI, the sub-Doppler-cooled ensemble is probed with photon recoils from stimulated Raman transitions where sequential pulses of the off-resonant 780 nm Raman beams coherently split, redirect, and combine atomic wave-packets to achieve matter-wave interference. Such lasers, components, and emitters can be fabricated using the silicon nitride platform. Phase shifts extracted from the interference can be related to inertial forces that the MOT experiences to extract, for example, local gravitational acceleration [27]. While the cooling and repump lasers generally require sub-megahertz integral linewidth (for resolving and locking to sat-spec) the requirements for the Raman laser are more stringent. The counter-propagating Raman beams probing the cloud must be phase coherent and any relative propagation delay due to laser frequency noise affects the interferometer sensitivity [44]. Their spatial beam profile and thereby the wavefront flatness also influences the sensitivity [130]. PIC-based beam intensity uniformity, measured to be <12% in 80% of the mode area in Ref. [43], is subject to fabrication tolerances and will require further beam profiling studies. AI experiments often use lower-noise bulky ECDL lasers as other semiconductor lasers may introduce noise contributions otherwise dominated by sensor vibration noise [131]. Significant efforts have been made toward developing compact laser systems for atom interferometry, including demonstrations of "single seed laser" operation with multiple modulators for generating and probing the MOT [27,132] as shown in Fig. 7(b). This has been achieved with frequency-doubled low-noise 1560 nm lasers with silicon photonics modulators [27] and with bulk-optic single-sideband modulators. In a direct-drive 780 nm AI-system-on-chip, using the laser and photonics technologies described in this paper, one

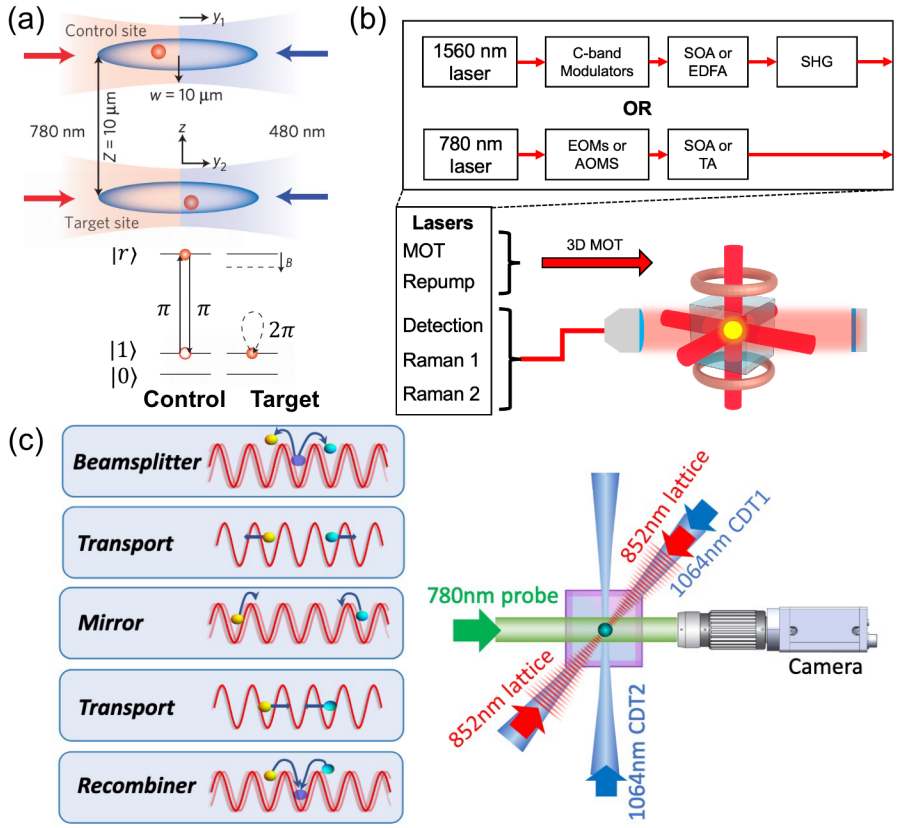

Fig. 7. Summary of MOT experiment applications. (a) Rydberg blockade interactions in a Rb MOT [125], reprinted [Figs. 1(a) and 1(b)] from E. Urban *et al.* Nature Phys 5, 110–114 (2009) with permission from Springer Nature. (b) Schematic for the single-laser MOT and AI system using frequency-doubling and silicon photonics modulators [27]. (c) Optical lattice AI [133], adapted from C. Ledesma et al, arXiv:2305.17603 (2023), with permission from the authors.

can envision using tunable photonic-integrated reference cavities for precisely controlling laser frequency and high extinction ratio, modulated, multi-ring filters as shutters [76,108]. These building blocks can form the basis for more integrated components specific to more complex AI demonstrations such as optical lattice AIs [126] based on ultra-cold BECs which require additional beams for cross dipole traps. With an optical lattice atom interferometer architecture [119], various lasers as shown in Fig. 7(c) are required for a cross-dipole lattice trap, where frequency shifting of counter propagating beams relative to each other provide the moving grating used for the shaking function. Other lasers are used to create the cold atom BEC and must be sequenced with the cross-dipole trap to realize the functions of beam splitter, interferometer arm transport, mirror, and recombining.

10. DISCUSSION AND FUTURE PROSPECTS

With recent advances in visible light to IR photonic integration technology, 3D-MOTs, one of the primary tools for creating large populations of cold atoms for quantum and atomic experiments, are poised to undergo a major transformation. The performance and degree of integration possible today can move the laser, optics, and functional building blocks of the 3D-MOT as well as the MOT itself to the chip scale. Such advances will enable portable, compact cold-atom experiments and greatly improve the reliability and scalability of a wide range of atomic, molecular, and AMO tools. In this paper, we reviewed the basics components and functions of the MOT and the potential for integration of the laser and optics portion of the 3D-MOT using the ultra-low loss silicon nitride platform and touched briefly on advances in miniaturization of atom generation and vacuum cell technology in the context of creating rubidium cold atoms.

Key challenges for these photonic integration technologies include expanding wavelength operation down to 200 nm to enable production a wider range of cold-atom species and further loss reduction at the lower end of visible wavelengths. Different wide bandgap material systems, such as tantalum pentoxide (tantala) and aluminum oxide (alumina) have made progress in loss reduction and demonstration of lasers and other simple building blocks. The silicon nitride platform as of today is more mature and capable of realizing the complex building blocks and complete integration of the MOT. Realization of high-power (>500 mW) integrated lasers is important for accessing certain transitions and cooling and trapping certain atomic species. Examples of this include the two-photon Rb transition requiring over 10 mW delivered to the atoms [66] as well as optical lattices for certain types of atom interferometers which may require over 10 W at 1064 nm [134]. In order to improve quantum experiment sensitivity, it is often required to increase the number of cooled atoms, and larger grating beam emitters over 6 mm are desirable. However, such increased grating sizes pose numerous challenges related to fabrication. Realizing grating emitters at shorter wavelengths toward the UV pushes the limits

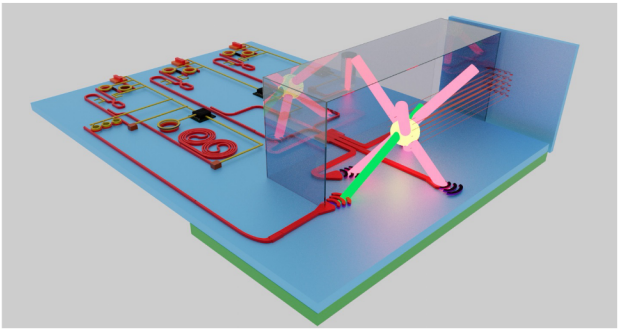

Fig. 8. Integrated photonic-atomic system interfaced with an optical tweezer chip containing an array of small focusing grating emitters.

of today's wafer-scale photonic lithography processes. Remaining challenges include attaching micro-atomic cells to photonic integrated circuits, further integrating atomic sources and vacuum into the chip, and integrated atom fluorescence detection and imaging. As the complexity of controlling all functions on a single chip increase, machine learning algorithms may become increasingly important [135]. Other transformative extensions can include planar optical integrated optical tweezer arrays [136] to trap individual atoms formed in the 3D-MOT as illustrated in Fig. 8. Due to the large silicon nitride transparency window of 405 nm–2350 nm [36], the PIC can be modified to work with other wavelengths by changing the waveguide width in the nitride patterning lithography mask, opening the potential to scaling to other atom species including cesium, strontium, barium, calcium, and ytterbium. By translating today's 3D-MOT table-top lasers and optical infrastructure to the chip scale, the reliability, scalability, and compactness of this critical heart of QIS experiments can be transformed. New photonic integration will also enable augmenting these compact 3D-MOTs with additional experimental chip-scale apparatus for further atomic trapping and manipulation stages for compute, sensing and other atomic applications, as well as the potential to control atoms in ways not possible with table-top, bulk-optic free space optics.

Funding. Air Force Research Laboratory (FA9453-20-2-0001); National Aeronautics and Space Administration (NASA) Quantum Pathways Institute (80NSSC23K1343); DARPA Microsystems Technology Office (FA9453-19-C-0030).

Acknowledgment. The authors wish to acknowledge James McGilligan (University of Strathclyde), Matthew Hummon and John Kitching (NIST), and Paul Kunz (ARL) for helpful feedback and discussions; Ryan Rudy (ARL) for contributions in PZT modulators; and Karl D. Nelson and Matthew W. Puckett (Honeywell Aerospace) for contributions to the grating emitter photonic design and silicon nitride wafer processing. We also thank Abigail Shull for help with creation and implementation of CAD drawings and figures. This material is based upon work supported by the NASA Quantum Pathways Institute (QPI) under grant number 80NSSC23K1343, Air Force Research Laboratory under grant number FA9453-20-2-0001, and DARPA Microsystems Technology Office under APHI contract number FA9453-19-C-0030. Any opinions, findings, and conclusions or recommendations expressed in this material are those of the author(s) and do not necessarily reflect the views of the National Aeronautics and Space Administration (NASA), the Department of Defense or the Defense Advanced Research Project Agency (DARPA), the Air Force Research Laboratory (AFRL), or the U.S. Government.

Disclosures. D.J.B., Infleqtion (FICPRS); A.I., Infleqtion (R); N.C., Infleqtion (R).

Data availability. Data underlying the results presented in this paper are not publicly available at this time but may be obtained from the authors upon reasonable request.

REFERENCES

1. W. B. Cairncross and J. Ye, "Atoms and molecules in the search for time-reversal symmetry violation," Nat. Rev. Phys. **1**, 510–521 (2019).
2. A. M. Kaufman and K.-K. Ni, "Quantum science with optical tweezer arrays of ultracold atoms and molecules," Nat. Phys. **17**, 1324–1333 (2021).
3. A. D. Ludlow, M. M. Boyd, J. Ye, *et al.*, "Optical atomic clocks," Rev. Mod. Phys. **87**, 637–701 (2015).
4. M. A. Norcia, A. W. Young, W. J. Eckner, *et al.*, "Seconds-scale coherence on an optical clock transition in a tweezer array," Science **366**, 93–97 (2019).
5. E. Pedrozo-Peñafiel, S. Colombo, C. Shu, *et al.*, "Entanglement on an optical atomic-clock transition," Nature **588**, 414–418 (2020).
6. J. Ye, H. J. Kimble, and H. Katori, "Quantum state engineering and precision metrology using state-insensitive light traps," Science **320**, 1734–1738 (2008).
7. C. L. Degen, F. Reinhard, and P. Cappellaro, "Quantum sensing," Rev. Mod. Phys. **89**, 035002 (2017).
8. D. C. Aveline, J. R. Williams, E. R. Elliott, *et al.*, "Observation of Bose–Einstein condensates in an Earth-orbiting research lab," Nature **582**, 193–197 (2020).
9. A. Larrouy, E. K. Dietsche, R. Richaud, *et al.*, "Quantum sensing using Rydberg atoms," in *Quantum Information and Measurement (QIM) V: Quantum Technologies* (OSA, 2019), p. S3A.5.
10. D. H. Meyer, Z. A. Castillo, K. C. Cox, *et al.*, "Assessment of Rydberg atoms for wideband electric field sensing," J. Phys. B: At. Mol. Opt. Phys. **53**, 034001 (2020).
11. J. Kitching, S. Knappe, and E. A. Donley, "Atomic sensors – a review," IEEE Sens. J. **11**, 1749–1758 (2011).
12. T. M. Graham, Y. Song, J. Scott, *et al.*, "Multi-qubit entanglement and algorithms on a neutral-atom quantum computer," Nature **604**, 457–462 (2022).
13. D. Bluvstein, H. Levine, G. Semeghini, *et al.*, "A quantum processor based on coherent transport of entangled atom arrays," Nature **604**, 451–456 (2022).
14. S. J. Evered, D. Bluvstein, M. Kalinowski, *et al.*, "High-fidelity parallel entangling gates on a neutral-atom quantum computer," Nature **622**, 268–272 (2023).
15. E. L. Raab, M. Prentiss, A. Cable, *et al.*, "Trapping of neutral sodium atoms with radiation pressure," Phys. Rev. Lett. **59**, 2631–2634 (1987).
16. K. Dieckmann, R. J. C. Spreeuw, M. Weidemüller, *et al.*, "Two-dimensional magneto-optical trap as a source of slow atoms," Phys. Rev. A **58**, 3891–3895 (1998).
17. J. P. McGilligan, K. Gallacher, P. F. Griffin, *et al.*, "Micro-fabricated components for cold atom sensors," Rev. Sci. Instrum. **93**, 091101 (2022).
18. H. J. Metcalf and P. Van der Straten, *Laser Cooling and Trapping* (Springer Science & Business Media, 1999).
19. A. Urvoy, Z. Vendeiro, J. Ramette, *et al.*, "Direct laser cooling to bose-einstein condensation in a dipole trap," Phys. Rev. Lett. **122**, 203202 (2019).
20. K. Frye, S. Abend, W. Bartosch, *et al.*, "The Bose-Einstein condensate and cold atom laboratory," EPJ Quantum Technol. **8**, 1–38 (2021).
21. A. L. Shaw, P. Scholl, R. Finklestein, *et al.*, "Dark-state enhanced loading of an optical tweezer array," Phys. Rev. Lett. **130**, 193402 (2023).
22. D. Barredo, S. De Léséleuc, V. Lienhard, *et al.*, "An atom-by-atom assembler of defect-free arbitrary two-dimensional atomic arrays," Science **354**, 1021–1023 (2016).
23. M. Schlosser, S. Tichelmann, D. Schäffner, *et al.*, "Scalable multi-layer architecture of assembled single-atom qubit arrays in a three-dimensional talbot tweezer lattice," Phys. Rev. Lett. **130**, 180601 (2023).

24. T. Müller, T. Wendrich, M. Gilowski, *et al.*, "Versatile compact atomic source for high-resolution dual atom interferometry," Phys. Rev. A **76**, 063611 (2007).
25. K. Bongs, M. Holynski, J. Vovrosh, *et al.*, "Taking atom interferometric quantum sensors from the laboratory to real-world applications," Nat. Rev. Phys. **1**, 731–739 (2019).
26. E. Di Gaetano, S. Watson, E. McBrearty, *et al.*, "Sub-megahertz linewidth 780.24 nm distributed feedback laser for ^{87}Rb applications," Opt. Lett. **45**, 3529–3532 (2020).
27. J. Lee, R. Ding, J. Christensen, *et al.*, "A compact cold-atom interferometer with a high data-rate grating magneto-optical trap and a photonic-integrated-circuit-compatible laser system," Nat. Commun. **13**, 5131 (2022).
28. A. Kodigala, M. Gehl, G. W. Hoth, *et al.*, "High-performance silicon photonic single-sideband modulators for cold-atom interferometry," Sci. Adv. **10**, eade4454 (2024).
29. W. Zhang, L. Stern, D. Carlson, *et al.*, "Ultranarrow linewidth photonic-atomic laser," Laser Photonics Rev. **14**, 1900293 (2020).
30. C. A. McLemore, N. Jin, M. L. Kelleher, *et al.*, "Miniaturizing ultrastable electromagnetic oscillators: sub-10^{-14}frequency instability from a centimeter-scale Fabry-Perot cavity," Phys. Rev. Appl. **18**, 054054 (2022).
31. N. Jin, C. A. McLemore, D. Mason, *et al.*, "Micro-fabricated mirrors with finesse exceeding one million," Optica **9**, 965–970 (2022).
32. C. C. Nshii, M. Vangeleyn, J. P. Cotter, *et al.*, "A surface-patterned chip as a strong source of ultracold atoms for quantum technologies," Nat. Nanotechnol. **8**, 321–324 (2013).
33. J. P. McGilligan, P. F. Griffin, R. Elvin, *et al.*, "Grating chips for quantum technologies," Sci. Rep. **7**, 384 (2017).
34. L. Chen, C.-J. Huang, X.-B. Xu, *et al.*, "Planar-integrated magneto-optical trap," Phys. Rev. Appl. **17**, 034031 (2022).
35. C. Ropp, W. Zhu, A. Yulaev, *et al.*, "Integrating planar photonics for multi-beam generation and atomic clock packaging on chip," Light: Sci. Appl. **12**, 83 (2023).
36. D. J. Blumenthal, "Photonic integration for UV to IR applications," APL Photonics **5**, 020903 (2020).
37. Z. L. Newman, V. Maurice, T. Drake, *et al.*, "Architecture for the photonic integration of an optical atomic clock," Optica **6**, 680–685 (2019).
38. M. Vangeleyn, P. F. Griffin, E. Riis, *et al.*, "Laser cooling with a single laser beam and a planar diffractor," Opt. Lett. **35**, 3453–3455 (2010).
39. S. Pollock, J. P. Cotter, A. Laliotis, *et al.*, "Characteristics of integrated magneto-optical traps for atom chips," New J. Phys. **13**, 043029 (2011).
40. Q. Bodart, S. Merlet, N. Malossi, *et al.*, "A cold atom pyramidal gravimeter with a single laser beam," Appl. Phys. Lett. **96**, 134101 (2010).
41. C. Ropp, A. Yulaev, D. Westly, *et al.*, "Meta-grating outcouplers for optimized beam shaping in the visible," Opt. Express **29**, 14789–14798 (2021).
42. N. Chauhan, D. Bose, M. Puckett, *et al.*, "Photonic integrated Si3N4 ultra-large-area grating waveguide MOT interface for 3D atomic clock laser cooling," in *Conference on Lasers and Electro-Optics (2019)* (Optica Publishing Group, 2019), p. STu4O.3.
43. A. Isichenko, N. Chauhan, D. Bose, *et al.*, "Photonic integrated beam delivery for a rubidium 3D magneto-optical trap," Nat. Commun. **14**, 3080 (2023).
44. J. Le Gouët, P. Cheinet, J. Kim, *et al.*, "Influence of lasers propagation delay on the sensitivity of atom interferometers," Eur. Phys. J. D **44**, 419–425 (2007).
45. M. L. Day, P. J. Low, B. White, *et al.*, "Limits on atomic qubit control from laser noise," npj Quantum Inf. **8**, 72 (2022).
46. D. J. Blumenthal, R. Heideman, D. Geuzebroek, *et al.*, "Silicon nitride in silicon photonics," Proc. IEEE **106**, 2209–2231 (2018).
47. X. Xu, T. H. Loftus, J. L. Hall, *et al.*, "Cooling and trapping of atomic strontium," J. Opt. Soc. Am. B **20**, 968 (2003).
48. G. W. Hoth, E. A. Donley, and J. Kitching, "Atom number in magneto-optic traps with millimeter scale laser beams," Opt. Lett. **38**, 661 (2013).
49. J. A. Rushton, M. Aldous, and M. D. Himsworth, "Contributed review: the feasibility of a fully miniaturized magneto-optical trap for portable ultracold quantum technology," Rev. Sci. Instrum. **85**, 121501 (2014).
50. P. D. Lett, R. N. Watts, C. I. Westbrook, *et al.*, "Observation of atoms laser cooled below the Doppler limit," Phys. Rev. Lett. **61**, 169–172 (1988).
51. A. J. Kerman, V. Vuletić, C. Chin, *et al.*, "Beyond optical molasses: 3D Raman sideband cooling of atomic cesium to high phase-space density," Phys. Rev. Lett. **84**, 439–442 (2000).
52. A. M. Kaufman, B. J. Lester, and C. A. Regal, "Cooling a single atom in an optical tweezer to its quantum ground state," Phys. Rev. X **2**, 041014 (2012).
53. F. Schreck and K. v. Druten, "Laser cooling for quantum gases," Nat. Phys. **17**, 1296–1304 (2021).
54. L. Zhu, X. Liu, B. Sain, *et al.*, "A dielectric metasurface optical chip for the generation of cold atoms," Sci. Adv. **6**, eabb6667 (2020).
55. K. I. Lee, J. A. Kim, H. R. Noh, *et al.*, "Single-beam atom trap in a pyramidal and conical hollow mirror," Opt. Lett. **21**, 1177–1179 (1996).
56. J. M. Kohel, J. Ramirez-Serrano, R. J. Thompson, *et al.*, "Generation of an intense cold-atom beam from a pyramidal magneto-optical trap: experiment and simulation," J. Opt. Soc. Am. B **20**, 1161–1168 (2003).
57. J. P. McGilligan, K. R. Moore, A. Dellis, *et al.*, "Laser cooling in a chip-scale platform," Appl. Phys. Lett. **117**, 054001 (2020).
58. W. R. McGehee, W. Zhu, D. S. Barker, *et al.*, "Magneto-optical trapping using planar optics," New J. Phys. **23**, 013021 (2021).
59. A. R. Ferdinand, Z. L. Newman, W. Zhu, *et al.*, "A scalable infrastructure for strontium optical clocks," in *Conference on Lasers and Electro-Optics (2022)* (Optica Publishing Group, 2022), p. STu5O.1.
60. K. K. Mehta, C. D. Bruzewicz, R. McConnell, *et al.*, "Integrated optical addressing of an ion qubit," Nat. Nanotechnol. **11**, 1066–1070 (2016).
61. R. J. Niffenegger, J. Stuart, C. Sorace-Agaskar, *et al.*, "Integrated multi-wavelength control of an ion qubit," Nature **586**, 538–542 (2020).
62. S. Kim, D. A. Westly, B. J. Roxworthy, *et al.*, "Photonic waveguide to free-space Gaussian beam extreme mode converter," Light: Sci. Appl. **7**, 72 (2018).
63. S. Jammi, A. R. Ferdinand, Z. Luo, *et al.*, "Three-dimensional, multi-wavelength beam formation with integrated metasurface optics for Sr laser cooling," Opt. Lett. **49**, 6013 (2024).
64. L. K. Heki, R. Chao, A. Isichenko, *et al.*, "High efficiency large-angle polarization-insensitive retroreflecting metasurface for magneto-optical traps," Appl. Phys. Lett. **124**, 251704 (2024).
65. R. Folman, P. Krüger, D. Cassettari, *et al.*, "Controlling cold atoms using nanofabricated surfaces: atom chips," Phys. Rev. Lett. **84**, 4749–4752 (2000).
66. Z. L. Newman, V. Maurice, C. Fredrick, *et al.*, "High-performance, compact optical standard," Opt. Lett. **46**, 4702 (2021).
67. G. J. Dick, "Local oscillator induced instabilities in trapped ion frequency standards," in *Proceedings of the 19th Annual Precise Time and Time Interval Systems and Applications Meeting* (1989), pp. 133–147.
68. J. Alnis, A. Schliesser, C. Y. Wang, *et al.*, "Thermal-noise-limited crystalline whispering-gallery-mode resonator for laser stabilization," Phys. Rev. A **84**, 011804 (2011).
69. A. B. Matsko, A. A. Savchenkov, N. Yu, *et al.*, "Whispering-gallery-mode resonators as frequency references I Fundamental limitations," J. Opt. Soc. Am. B **24**, 1324 (2007).
70. J. H. Dallyn, K. Liu, M. W. Harrington, *et al.*, "Thermal and driven noise in Brillouin lasers," Phys. Rev. A **105**, 043506 (2022).
71. P. R. Stanfield, A. J. Leenheer, C. P. Michael, *et al.*, "CMOS-compatible, piezo-optomechanically tunable photonics for visible wavelengths and cryogenic temperatures," Opt. Express **27**, 28588–28605 (2019).
72. M. Yu, R. Cheng, C. Reimer, *et al.*, "Integrated electro-optic isolator on thin-film lithium niobate," Nat. Photonics **17**, 666–671 (2023).
73. E. A. Kittlaus, W. M. Jones, P. T. Rakich, *et al.*, "Electrically driven acousto-optics and broadband non-reciprocity in silicon photonics," Nat. Photonics **15**, 43–52 (2021).

74. E. A. Kittlaus, N. T. Otterstrom, and P. T. Rakich, "On-chip inter-modal Brillouin scattering," Nat. Commun. **8**, 15819 (2017).
75. K. Liu, N. Chauhan, M. Song, *et al.*, "Tunable broadband two-point-coupled ultra-high-*Q* visible and near-infrared photonic integrated resonators," Photonics Res. **12**, 1890–1898 (2024).
76. J. Wang, K. Liu, M. W. Harrington, *et al.*, "Silicon nitride stress-optic microresonator modulator for optical control applications," Opt. Express **30**, 31816–31827 (2022).
77. M. T. Hummon, S. Kang, D. G. Bopp, *et al.*, "Photonic chip for laser stabilization to an atomic vapor with 10^{-11} instability," Optica **5**, 443–449 (2018).
78. G. Moille, D. Westly, and K. Srinivasan, "Broadband visible wavelength microcomb generation in silicon nitride microrings through air-clad dispersion engineering," arXiv (2024).
79. B. Li, Z. Yuan, W. Jin, *et al.*, "High-coherence hybrid-integrated 780 nm source by self-injection-locked second-harmonic generation in a high-Q silicon-nitride resonator," Optica **10**, 1241–1244 (2023).
80. X. Lu, G. Moille, A. Singh, *et al.*, "Milliwatt-threshold visible–telecom optical parametric oscillation using silicon nanophotonics," Optica **6**, 1535–1541 (2019).
81. E. Trageser, H. Zhang, S. Palmer, *et al.*, "Blue GaN-based DFB laser diode with sub-MHz linewidth," Opt. Express **32**, 23372–23380 (2024).
82. N. Goossen-Schmidt, C. Pyrlik, M. T. Hassan, *et al.*, "High power distributed Bragg reflector lasers at 689.45 nm for quantum technology applications," IEEE Photonics Technol. Lett. **34**, 679–682 (2022).
83. Z. Zhang, B. Shen, M. A. Tran, *et al.*, "Photonic integration platform for rubidium sensors and beyond," Optica **10**, 752–753 (2023).
84. D. Huang, M. A. Tran, J. Guo, *et al.*, "High-power sub-kHz linewidth lasers fully integrated on silicon," Optica **6**, 745–752 (2019).
85. A. Siddharth, A. Attanasio, S. Bianconi, *et al.*, "Piezoelectrically tunable, narrow linewidth photonic integrated extended-DBR lasers," Optica **11**, 1062–1069 (2024).
86. H. Wenzel, B. Arar, A. Maaßdorf, *et al.*, "Distributed Bragg reflector lasers emitting between 696 and 712 nm," Electron. Lett. **58**, 908–910 (2022).
87. P. A. Morton and M. J. Morton, "High-power, ultra-low noise hybrid lasers for microwave photonics and optical sensing," J. Lightwave Technol. **36**, 5048–5057 (2018).
88. Y. Lin, C. Browning, R. B. Timens, *et al.*, "Narrow linewidth hybrid InP-TriPleX photonic integrated tunable laser based on silicon nitride micro-ring resonators," in 2018 Optical Fiber Communications Conference and Exposition (OFC) (2018), pp. 1–3.
89. Y.-H. Lai, D. Eliyahu, S. Ganji, *et al.*, "780 nm narrow-linewidth self-injection-locked WGM lasers," in *Laser Resonators, Microresonators, and Beam Control XXII*, Vol. 11266 (SPIE, 2020), pp. 78–84.
90. A. L. Schawlow and C. H. Townes, "Infrared and optical masers," Phys. Rev. **112**, 1940–1949 (1958).
91. M. Corato-Zanarella, A. Gil-Molina, X. Ji, *et al.*, "Widely tunable and narrow-linewidth chip-scale lasers from near-ultraviolet to near-infrared wavelengths," Nat. Photonics **17**, 157–164 (2023).
92. W. Jin, Q.-F. Yang, L. Chang, *et al.*, "Hertz-linewidth semiconductor lasers using CMOS-ready ultra-high-Q microresonators," Nat. Photonics **15**, 346–353 (2021).
93. M. W. Puckett, K. Liu, N. Chauhan, *et al.*, "422 mMillion intrinsic quality factor planar integrated all-waveguide resonator with sub-MHz linewidth," Nat. Commun. **12**, 934 (2021).
94. A. Isichenko, A.S. Hunter, D. Bose, *et al.*, "Sub-Hz fundamental, sub-kHz integral linewidth self-injection locked 780 nm hybrid integrated laser," Sci. Rep. **14**, 27015 (2024).
95. S. Gundavarapu, G. M. Brodnik, M. Puckett, *et al.*, "Sub-hertz fundamental linewidth photonic integrated Brillouin laser," Nat. Photonics **13**, 60–67 (2019).
96. N. Chauhan, A. Isichenko, K. Liu, *et al.*, "Visible light photonic integrated Brillouin laser," Nat. Commun. **12**, 4685 (2021).
97. A. Isichenko, N. Chauhan, J. Wang, *et al.*, "Frequency modulated integrated 780 nm Brillouin laser with 24 Hz fundamental and 1.4 kHz integral linewidths and 22 kHz modulation bandwidth," in *Optical Fiber Communication Conference (OFC) 2024* (Optica Publishing Group, 2024), p. W3D.2.
98. N. Chauhan, C. Caron, J. Wang, *et al.*, "Trapped ion qubit and clock operations with a visible wavelength photonic coil resonator stabilized integrated Brillouin laser," arXiv (2024).
99. N. Chauhan, "Stabilized Sources in Visible for Atomic, Molecular and Quantum Applications," Ph.D. dissertation (University of California, Santa Barbara, 2024).
100. A. D. White, G. H. Ahn, K. V. Gasse, *et al.*, "Integrated passive nonlinear optical isolators," Nat. Photonics **17**, 143–149 (2023).
101. M. Harfouche, D. Kim, H. Wang, *et al.*, "Kicking the habit/semiconductor lasers without isolators," Opt. Express **28**, 36466–36475 (2020).
102. C. Xiang, W. Jin, O. Terra, *et al.*, "3D integration enables ultralow-noise isolator-free lasers in silicon photonics," Nature **620**, 78–85 (2023).
103. J. Ye, S. Swartz, P. Jungner, *et al.*, "Hyperfine structure and absolute frequency of the ^{87}Rb $5P_{3/2}$ state," Opt. Lett. **21**, 1280–1282 (1996).
104. D. Renaud, D. R. Assumpcao, G. Joe, *et al.*, "Sub-1 Volt and high-bandwidth visible to near-infrared electro-optic modulators," Nat. Commun. **14**, 1496 (2023).
105. A. N. R. Ahmed, A. Mercante, S. Shi, *et al.*, "Vertical mode transition in hybrid lithium niobate and silicon nitride-based photonic integrated circuit structures," Opt. Lett. **43**, 4140–4143 (2018).
106. L. Shao, D. Zhu, M. Colangelo, *et al.*, "Electrical control of surface acoustic waves," Nat. Electron. **5**, 348–355 (2022).
107. E. A. Kittlaus, N. T. Otterstrom, P. Kharel, *et al.*, "Non-reciprocal interband Brillouin modulation," Nat. Photonics **12**, 613–619 (2018).
108. T. A. Huffman, G. M. Brodnik, C. Pinho, *et al.*, "Integrated resonators in an ultralow loss Si_3N_4/SiO_2platform for multifunction applications," IEEE J. Sel. Top. Quantum Electron. **24**, 1–9 (2018).
109. R. W. P. Drever, J. L. Hall, F. V. Kowalski, *et al.*, "Laser phase and frequency stabilization using an optical resonator," Appl. Phys. B **31**, 97–105 (1983).
110. K. Liu, J. H. Dallyn, G. M. Brodnik, *et al.*, "Photonic circuits for laser stabilization with integrated ultra-high Q and Brillouin laser resonators," APL Photonics **7**, 096104 (2022).
111. K. Liu, N. Chauhan, J. Wang, *et al.*, "36 Hz integral linewidth laser based on a photonic integrated 4.0 m coil resonator," Optica **9**, 770–775 (2022).
112. B. Li, W. Jin, L. Wu, *et al.*, "Reaching fiber-laser coherence in integrated photonics," Opt. Lett. **46**, 5201–5204 (2021).
113. Y. Lin, Z. Yong, X. Luo, *et al.*, "Monolithically integrated, broadband, high-efficiency silicon nitride-on-silicon waveguide photodetectors in a visible-light integrated photonics platform," Nat. Commun. **13**, 6362 (2022).
114. S. Feng, Y. Geng, K. M. Lau, *et al.*, "Epitaxial III–V-on-silicon waveguide butt-coupled photodetectors," in *The 9th International Conference on Group IV Photonics (GFP)* (2012), pp. 51–53.
115. Q. Yu, J. Gao, N. Ye, *et al.*, "Heterogeneous photodiodes on silicon nitride waveguides," Opt. Express **28**, 14824–14830 (2020).
116. M. Jahed, A. Caut, J. Goyvaerts, *et al.*, "Angled flip-chip integration of VCSELs on silicon photonic integrated circuits," J. Lightwave Technol. **40**, 5190–5200 (2022).
117. Y. Kang, M. Zadka, S. Litski, *et al.*, "Epitaxially-grown Ge/Si avalanche photodiodes for 1.3 μm light detection," Opt. Express **16**, 9365–9371 (2008).
118. N. Chauhan, J. Wang, D. Bose, *et al.*, "Ultra-low loss visible light waveguides for integrated atomic, molecular, and quantum photonics," Opt. Express **30**, 6960–6969 (2022).
119. B. Desiatov, A. Shams-Ansari, M. Zhang, *et al.*, "Ultra-low-loss integrated visible photonics using thin-film lithium niobate," Optica **6**, 380–384 (2019).
120. J. Kitching, "Chip-scale atomic devices," Appl. Phys. Rev. **5**, 031302 (2018).
121. T. Grzebyk, A. Górecka-Drzazga, and J. A. Dziuban, "Glow-discharge ion-sorption micropump for vacuum MEMS," Sens. Actuators, Phys. **208**, 113–119 (2014).
122. L. Liu, D.-S. Lü, W.-B. Chen, *et al.*, "In-orbit operation of an atomic clock based on laser-cooled ^{87}Rb atoms," Nat. Commun. **9**, 2760 (2018).

123. D. Bose, M. W. Harrington, A. Isichenko, *et al.*, "Anneal-free ultra-low loss silicon nitride integrated photonics," Light: Sci. Appl. **13**, 156 (2024).
124. W. Loh, J. Stuart, D. Reens, *et al.*, "Operation of an optical atomic clock with a Brillouin laser subsystem," Nature **588**, 244–249 (2020).
125. E. Urban, T. A. Johnson, T. Henage, *et al.*, "Observation of Rydberg blockade between two atoms," Nat. Phys. **5**, 110–114 (2009).
126. C. A. Weidner, H. Yu, R. Kosloff, *et al.*, "Atom interferometry using a shaken optical lattice," Phys. Rev. A **95**, 043624 (2017).
127. B. Stray, A. Lamb, A. Kaushik, *et al.*, "Quantum sensing for gravity cartography," Nature **602**, 590–594 (2022).
128. M. Saffman, "Quantum computing with atomic qubits and Rydberg interactions: progress and challenges," J. Phys. B: At. Mol. Opt. Phys. **49**, 202001 (2016).
129. E. A. Burt, J. D. Prestage, R. L. Tjoelker, *et al.*, "Demonstration of a trapped-ion atomic clock in space," Nature **595**, 43–47 (2021).
130. N. Mielec, M. Altorio, R. Sapam, *et al.*, "Atom interferometry with top-hat laser beams," Appl. Phys. Lett. **113**, 161108 (2018).
131. X. Zhang, J. Zhong, B. Tang, *et al.*, "Compact portable laser system for mobile cold atom gravimeters," Appl. Opt. **57**, 6545 (2018).
132. S.-w. Chiow and N. Yu, "Compact atom interferometer using single laser," Appl. Phys. B **124**, 96 (2018).
133. C. LeDesma, K. Mehling, J. Shao, *et al.*, "A machine-designed optical lattice atom interferometer," Phys. Rev. Res. **6**, 043120 (2024).
134. C. LeDesma, K. Mehling, and M. Holland, "Vector atom accelerometry in an optical lattice," arXiv (2024).
135. A. D. Tranter, H. J. Slatyer, M. R. Hush, *et al.*, "Multiparameter optimisation of a magneto-optical trap using deep learning," Nat. Commun. **9**, 4360 (2018).
136. A. Cooper, J. P. Covey, I. S. Madjarov, *et al.*, "Alkaline-earth atoms in optical tweezers," Phys. Rev. X **8**, 041055 (2018).

https://doi.org/10.1364/OPTICAQ.517600